IL-1β–driven osteoclastogenic Tregs accelerate bone erosion in arthritis

Anaïs Levescot,[1] Margaret H. Chang,[1,2] Julia Schnell,[1,3] Nathan Nelson-Maney,[1] Jing Yan,[1,4] Marta Martínez-Bonet,[1] Ricardo Grieshaber-Bouyer,[1] Pui Y. Lee,[1,2] Kevin Wei,[1] Rachel B. Blaustein,[1] Allyn Morris,[1] Alexandra Wactor,[1] Yoichiro Iwakura,[5] James A. Lederer,[6] Deepak A. Rao,[1] Julia F. Charles,[1,4] and Peter A. Nigrovic[1,2]

[1]Division of Rheumatology, Inflammation, and Immunity, Brigham and Women's Hospital, Boston, Massachusetts, USA. [2]Division of Immunology, Boston Children's Hospital, Boston, Massachusetts, USA. [3]Department of Medicine V, Hematology, Oncology and Rheumatology, Heidelberg University Hospital, Heidelberg, Germany. [4]Department of Orthopaedic Surgery, Brigham and Women's Hospital, Boston, Massachusetts, USA. [5]Center for Experimental Animal Models, Research Institute for Science & Technology, Tokyo University of Science, Tokyo, Japan. [6]Department of Surgery, Brigham and Women's Hospital, Boston, Massachusetts, USA.

IL-1β is a proinflammatory mediator with roles in innate and adaptive immunity. Here we show that IL-1β contributes to autoimmune arthritis by inducing osteoclastogenic capacity in Tregs. Using mice with joint inflammation arising through deficiency of the IL-1 receptor antagonist (*Il1rn*$^{-/-}$), we observed that IL-1β blockade attenuated disease more effectively in early arthritis than in established arthritis, especially with respect to bone erosion. Protection was accompanied by a reduction in synovial CD4^{+}Foxp3^{+} Tregs that displayed preserved suppressive capacity and aerobic metabolism but aberrant expression of RANKL and a striking capacity to drive RANKL-dependent osteoclast differentiation. Both *Il1rn*$^{-/-}$ Tregs and wild-type Tregs differentiated with IL-1β accelerated bone erosion upon adoptive transfer. Human Tregs exhibited analogous differentiation, and corresponding RANKL^{hi}Foxp3^{+} T cells could be identified in rheumatoid arthritis synovial tissue. Together, these findings identify IL-1β–induced osteoclastogenic Tregs as a contributor to bone erosion in arthritis.

Introduction

IL-1 is a pleiotropic cytokine that plays a key role in the pathogenesis of inflammatory arthritis, including the highly prevalent disease rheumatoid arthritis (RA) and its less common pediatric counterpart juvenile idiopathic arthritis (1). Two members of the IL-1 subfamily, IL-1α and IL-1β, engage a broad program of pathways that promote inflammation, accelerate myeloid development, enhance expression of endothelial adhesion molecules, and activate hematopoietic and stromal lineages (2). Within the joint, IL-1 contributes to joint injury by stimulating release of degradative enzymes, including matrix metalloproteinases, cathepsins, and mast cell proteases (3). IL-1 also promotes the development of osteoclasts and thereby contributes to bone erosions that degrade joint function (4).

In animal models, the pivotal contribution of IL-1 to arthritis is reflected in the dense resistance of mice lacking IL-1 or its receptor to experimental arthritis, and the important role for IL-1 as an amplifier in T cell–mediated arthritis (5–7). In the BALB/c background, mice lacking the endogenous IL-1 receptor antagonist (IL-1Ra, encoded by *Il1rn*) rapidly develop highly inflammatory and destructive joint disease (8). *Il1rn*$^{-/-}$ arthritis affords an opportunity to dissect in detail the mechanisms by which unrestrained IL-1 activity causes joint disease. Perhaps surprisingly, lymphocytes represent major pathogenic actors; CD4^{+} T cells from *Il1rn*$^{-/-}$ donors induce arthritis in *nu/nu* mice by directing the traffic of IL-17–producing γδ T cells to the joint (9, 10). The cytokines IL-1β, TNF, and IL-17A are each essential to the evolution of the disease, while IL-1α, IL-6, and B cells are dispensable (9–13). *Il1rn*$^{-/-}$ arthritis thus contrasts mechanistically with collagen-induced arthritis and K/BxN arthritis, models in which joint inflammation is mediated primarily by immune complexes formed by autoantibodies, mirroring the division in human disease between immune complex–independent and immune complex–dependent arthritis (14).

Effector T (Teff) cell pathways have been well studied in *Il1rn*$^{-/-}$ arthritis, but the role of Tregs remains incompletely defined. Tregs are characterized by the signature transcription factor FOXP3 and play an essential role in suppressing autoimmunity (15). Mice require continuous *Foxp3* expression throughout life to avoid autoimmunity (16, 17). Tregs are enriched in inflamed human joints compared with peripheral blood, and murine studies confirm a role for Tregs in suppressing synovial inflammation (18–20). Beyond limiting the activity of Teff cells, Tregs can constrain joint destruction by directly inhibiting osteoclast development through contact-dependent and -independent mechanisms (20–22).

Intriguingly, environmental factors can convert Tregs into cells that promote rather than attenuate inflammatory pathology. In collagen-induced arthritis, IL-6 drives CD25^{lo}Foxp3^{+} Tregs to lose *Foxp3* expression and acquire both IL-17 and the osteoclast-differentiating factor receptor activator of NF-κB ligand (RANKL), becoming "exFoxp3" cells that accelerate bone erosion (23). Tregs can also be driven to express IL-17 while maintaining expression of *Foxp3*, including by exposure to IL-1, potentially rendering them

Conflict of interest: The authors have declared that no conflict of interest exists.

Submitted: June 3, 2020; **Accepted:** July 22, 2021; **Published:** September 15, 2021.
Reference information: *J Clin Invest*. 2021;131(18):e141008.
https://doi.org/10.1172/JCI141008.

pro- rather than antiinflammatory (24, 25). The role of IL-1 as a modulator of Treg function in arthritis remains unknown.

Using *Il1rn*$^{-/-}$ and Foxp3^{eGFP} *Il1rn*$^{-/-}$ animals, together with IL-1 inhibitors, we studied the course of *Il1rn*$^{-/-}$ arthritis. We found that early IL-1β blockade attenuated disease severity more effectively than delayed IL-1β blockade, in particular with respect to bone erosion. Unexpectedly, Foxp3-expressing *Il1rn*$^{-/-}$ Tregs developed expression of RANKL and a marked capacity to induce osteoclast differentiation, in a manner inhibited by IL-1β blockade. Adoptive transfer of *Il1rn*$^{-/-}$ Foxp3^{+}CD4^{+} T cells augmented bone erosion in a second model of arthritis, confirming their pathogenic capacity. WT Tregs differentiated in the presence of IL-1β acquired RANKL expression and osteoclastogenic function. Comparable pathogenic Tregs could be generated from human lymphocytes via IL-1β and were markedly expanded in human RA tissues. Together, these findings implicate Tregs driven by IL-1β to become osteoclastogenic Tregs (O-Tregs) as a to our knowledge previously undescribed mediator of bone erosion in autoimmune arthritis.

Results

Early administration of IL-1 blockade ameliorates swelling and bone erosion in arthritis. Il1rn$^{-/-}$ mice spontaneously develop arthritis in an IL-17– and T cell–dependent manner, reflecting the impact of uncontested IL-1β signaling on lymphocyte development and function (8). We used cytokine blockade to examine the time course of this process. Administration of a specific anti–IL-1β antibody early in disease, at time of weaning, led to a sustained improvement in arthritis, whereas IL-1β blockade administered after a 2-week delay only partially ameliorated disease (Figure 1, A and B). Histological analysis 6 weeks after weaning revealed that early IL-1β blockade was particularly effective for bone erosion (Figure 1, C and D and Supplemental Figure 1; supplemental material available online with this article; https://doi.org/10.1172/JCI141008DS1). The impact on bone was further confirmed by high-resolution x-ray micro-computed tomography (μCT), documenting a measurable reduction in bone injury only when cytokine blockade was initiated early in disease (Figure 1, E and F).

To understand the mechanism of this effect, we isolated synovial tissue cells from *Il1rn*$^{-/-}$ mice treated with isotype control, early anti–IL-1β, or late anti–IL-1β, followed by overnight stimulation with PMA/ionomycin to assess cytokine production by intracellular staining. *Il1rn*$^{-/-}$ CD4^{+} T cells exhibited both IL-17A and IFN-γ production, abrogated to a greater degree with early compared with late cytokine blockade, paralleling disease amelioration (Figure 1, G–I). To track the balance of Teff cells and Tregs, we generated *Il1rn*$^{-/-}$ × BALB/c Foxp3^{eGFP} mice. Paradoxically, the proportion of CD3^{+}CD4^{+}Foxp3^{+} cells increased in inflamed joints and decreased with treatment, especially if treatment was initiated early in the disease course (Figure 1J).

Highly suppressive Foxp3^{+} *Tregs are expanded in Il1rn*$^{-/-}$ *synovium.* Tregs from inflamed *Il1rn*$^{-/-}$ joints displayed the Th17 markers CCR6 and CD39 (Figure 2, A and B). However, stimulation with PMA/ionomycin failed to elicit production of IL-17A by *Il1rn*$^{-/-}$ Foxp3^{+} cells, whereas Foxp3^{-} T cells were strongly positive (Figure 2, C and D). Consistent with this result, *Il1rn*$^{-/-}$ Foxp3^{+} cells showed no expression of RORγt (Figure 2, E and F) and sorted *Il1rn*$^{-/-}$ Foxp3^{+} cells from lymph nodes exhibited no increase in expression of *Il17* mRNA (Supplemental Figure 2). Expression of CCR6 in the absence of IL-17 suggested anti-Th17 specialization rather than Th17 conversion (26). Studies of suppressive function supported this conclusion. Using lymph nodes as a cell source, sorted Tregs (CD3^{+}CD4^{+}Foxp3^{eGFP+}) from *Il1rn*$^{-/-}$ and WT mice were cocultured with Teff cells (CD3^{+}CD4^{+}Foxp3^{eGFP-}) from WT mice stained with CellTrace Violet to track proliferation by dye dilution after 72-hour stimulation with anti-CD3/anti-CD28 beads. Tregs from untreated *Il1rn*$^{-/-}$ mice exhibited suppressive capacity superior to that of WT Tregs, a difference neutralized by in vivo IL-1 blockade (Figure 2, G and H, and Supplemental Figure 3). Comparable findings were found when Tregs were incubated with Teff cells from the same donor type (Figure 2, I and J). Moreover, after 72 hours of stimulation in vitro we observed no loss of Foxp3 expression by *Il1rn*$^{-/-}$ Tregs (Supplemental Figure 4, A and B), suggesting that Foxp3 expression by these Tregs is stable, as shown in other contexts (27). Stability was further confirmed by adoptive transfer of Foxp3^{+} T cells into healthy recipient animals, finding in vivo persistence in blood and tissues for 1 week without significant differences in Foxp3 expression between WT and *Il1rn*$^{-/-}$ cells (Supplemental Figure 4, C and D). However, the ability of *Il1rn*$^{-/-}$ Tregs to convert conventional T cells into induced Tregs (sometimes termed "infectious tolerance") was slightly decreased compared with WT Tregs (Supplemental Figure 4, E and F). These findings confirm that the expanded *Il1rn*$^{-/-}$ Tregs do not represent a known population of pathogenic Tregs or exTregs.

A metabolic program associated with increased suppressive capacity in Il1rn$^{-/-}$ *Tregs.* To further evaluate the features of *Il1rn*$^{-/-}$ Tregs, we performed bulk RNA sequencing (RNA-seq) of Tregs from WT and *Il1rn*$^{-/-}$ lymph nodes. WT and *Il1rn*$^{-/-}$ Tregs showed similar expression of multiple genes associated with suppressor function, including *Foxp3*, *Il2ra*, *Il7r*, and *Ebi3* (a component of the suppressive cytokine IL-35), and transcription factors including *Eomes*, *Tbx21* (encoding Tbet), and *Irf4* (28). Tregs from WT and *Il1rn*$^{-/-}$ mice showed similar expression of genes encoding molecules involved in Treg localization and trafficking, including CXCR6, CXCR3, and CCR10 (Figure 3A). However, gene set enrichment analysis (GSEA) identified enhanced expression of genes encoding proteins involved in fatty acid metabolism (for example, NTHL1 and GABARAPL1) in *Il1rn*$^{-/-}$ Tregs and oxidative phosphorylation (OxPhos; for example, ATP5H and NDUFB3) in WT Tregs (Figure 3, B and C). To test the effect of these expression differences on cell metabolism, WT Foxp3^{+} and *Il1rn*$^{-/-}$ Foxp3^{+} T cells were cultured in the absence of glucose, glutamine, or lipids, and the extracellular acidification rate (ECAR), a measurement of lactate production, was determined upon readdition of glucose (Figure 3D). Consistent with GSEA data, *Il1rn*$^{-/-}$ Foxp3^{+} Tregs exhibited less of an increase in ECAR than WT Tregs. Oligomycin was then added to block mitochondrial ATP production and promote maximal rates of glycolysis. *Il1rn*$^{-/-}$ Foxp3^{+} Tregs showed a more robust increase in ECAR following oligomycin treatment than WT Tregs. These data indicate that WT Tregs perform glycolysis at maximal rates following glucose addition, with limited capacity to increase this pathway, consistent with published findings (29). By contrast, *Il1rn*$^{-/-}$ Foxp3^{+} Tregs exhibited greater glycolytic capacity and reserve than WT Tregs (Figure 3, D and E). This finding is consistent with the superiority of *Il1rn*$^{-/-}$ Tregs with

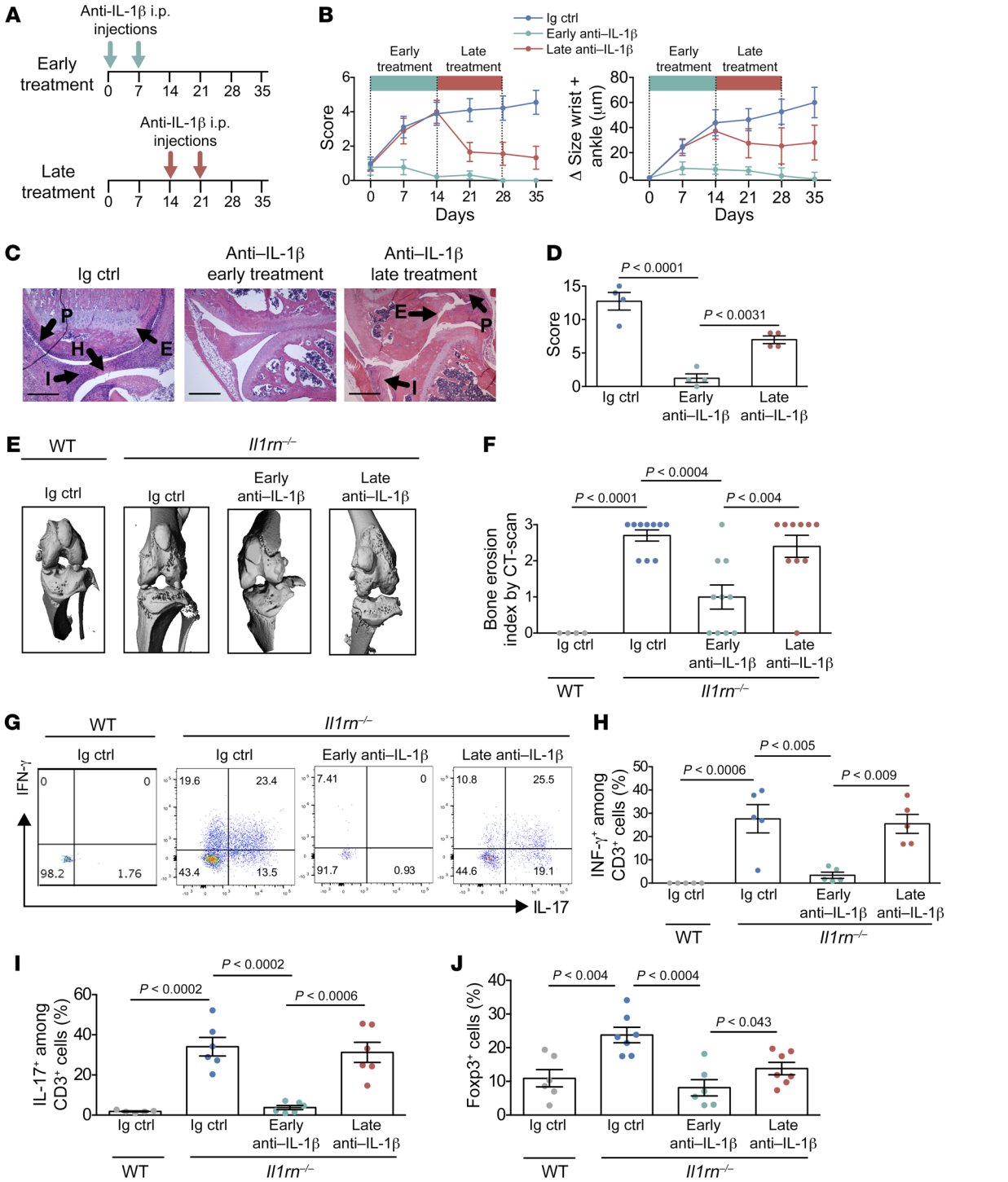

Figure 1. Attenuated bone erosion and Treg accumulation with early IL-1β blockade. (**A**–**I**) *Il1rn*$^{-/-}$ mice were treated with anti–IL-1β or isotype-matched IgG (n = 6) (5 mg/kg i.p. once per week) for 2 weeks either at the weaning (early treatment, n = 6) or 14 days after (late treatment n = 6). (**A**) Experimental scheme detailing administration time of i.p. anti–IL-1β. (**B**) Arthritis score (0–3/per paw, 0–12 total) and ankle and wrist thickening measured by calipers were followed for 35 days after arthritis weaning. (**C**) H&E staining of representative knee joints. *Il1rn*$^{-/-}$ joints from mice treated with isotype control or late anti–IL-1β display cellular infiltration (I), synovial hyperplasia (H), pannus formation (P), and bone and cartilage erosion (E). Scale bars: 1 μm. (**D**) Histological evaluation of knee joints from *Il1rn*$^{-/-}$ mice treated with anti–IL-1β (early treatment n = 4, late treatment n = 4) or isotype-matched IgG (n = 4). (**E**) High-resolution micro-computed tomography (μCT) imaging of knees from WT and *Il1rn*$^{-/-}$ mice treated with anti–IL-1β (n = 10 per group) or isotype-matched IgG (n = 4). (**F**) Bone erosion score by μCT (0–3 total). (**G**) Cytokine expression by CD3^{+}Foxp3^{eGFP+} cells from synovial tissue by flow cytometry. (**H** and **I**) Frequency of CD3^{+}Foxp3^{eGFP+} cells expressing IFN-γ and IL-17A. (**J**) Frequency of Foxp3^{eGFP+} cells among CD3^{+} cells in joint tissue. Data are expressed as mean ± SEM. Statistical significance was determined using 3-way ANOVA (**B**) or 1-way ANOVA (**D**, **F**, **G**, and **I**).

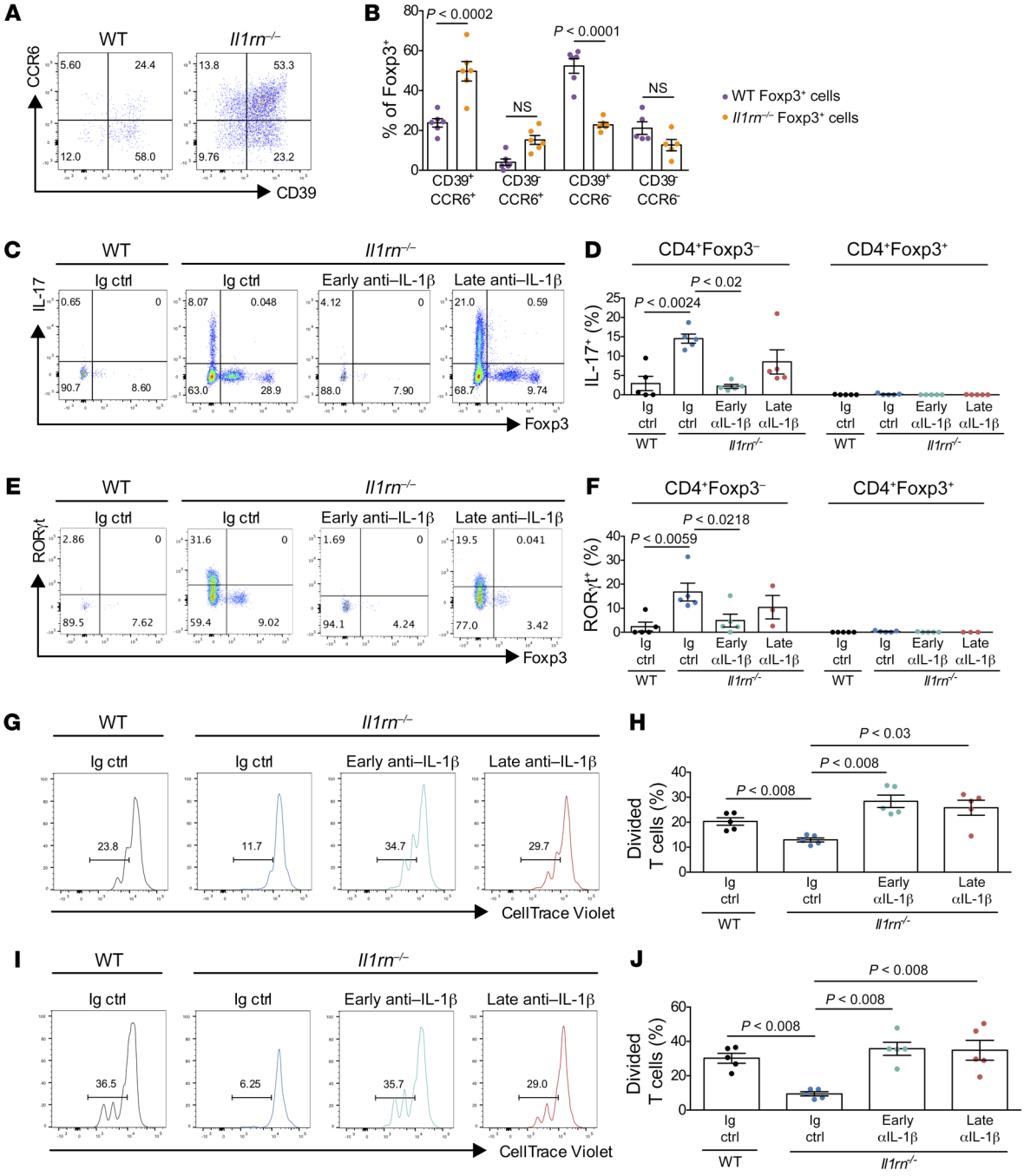

Figure 2. *Il1rn*$^{-/-}$ Tregs are present and highly suppressive. (**A**) CCR6 and CD39 expression on CD4$^+$Foxp3$^+$ T cells from WT and *Il1rn*$^{-/-}$ mouse synovial tissue by flow cytometry (n = 6). (**B**) Frequency of CD39 and CCR6 on Foxp3$^+$ T cells from synovial tissue. (**C**–**H**) *Il1rn*$^{-/-}$ mice were treated with anti–IL-1β (αIL-1β) or isotype-matched IgG (n = 5) (5 mg/kg i.p. once per week) for 2 weeks either at weaning (early treatment, n = 5) or 14 days after (late treatment n = 5). (**C**) Foxp3 and IL-17 expression by CD4$^+$ T cells from synovial tissue harvested 35 days after weaning by flow cytometry (n = 5). (**D**) Frequency of CD4$^+$Foxp3$^-$ and CD4$^+$Foxp3$^+$ cells expressing IL-17 from synovial tissue harvested 35 days after weaning (n = 5 per group). (**E**) Foxp3 and RORγt expression by CD4$^+$ cells from synovial tissue by flow cytometry (n = 5, late treatment n = 3). (**F**) Frequency of CD4$^+$Foxp3$^-$ and CD4$^+$Foxp3$^+$ cells expressing RORγt (n = 5 per group, late treatment n = 3). (**G** and **H**) Foxp3$^+$ cells from WT mice or *Il1rn*$^{-/-}$ mice treated with anti–IL-1β or isotype-matched IgG were cocultured with WT Foxp3$^-$ cells (n = 5 per group). (**G**) Proliferation of CD3$^+$Foxp3$^-$ cells following 72 hours of coculture. (**H**) Percentage of divided WT CD3$^+$Foxp3$^-$ cells. (**I** and **J**) Foxp3$^+$ cells from WT mice or *Il1rn*$^{-/-}$ mice treated with anti–IL-1β or isotype-matched IgG were cocultured with Foxp3^{eGFP-} cells from a donor of the same strain (n = 5 per group). (**I**) Foxp3$^-$ cell proliferation following 72 hours of coculture. (**J**) Percentage of divided WT Foxp3$^-$ cells. Data are expressed as mean ± SEM. Statistical significance was determined using 1-way ANOVA (**B**, **D**, **F**, and **H**).

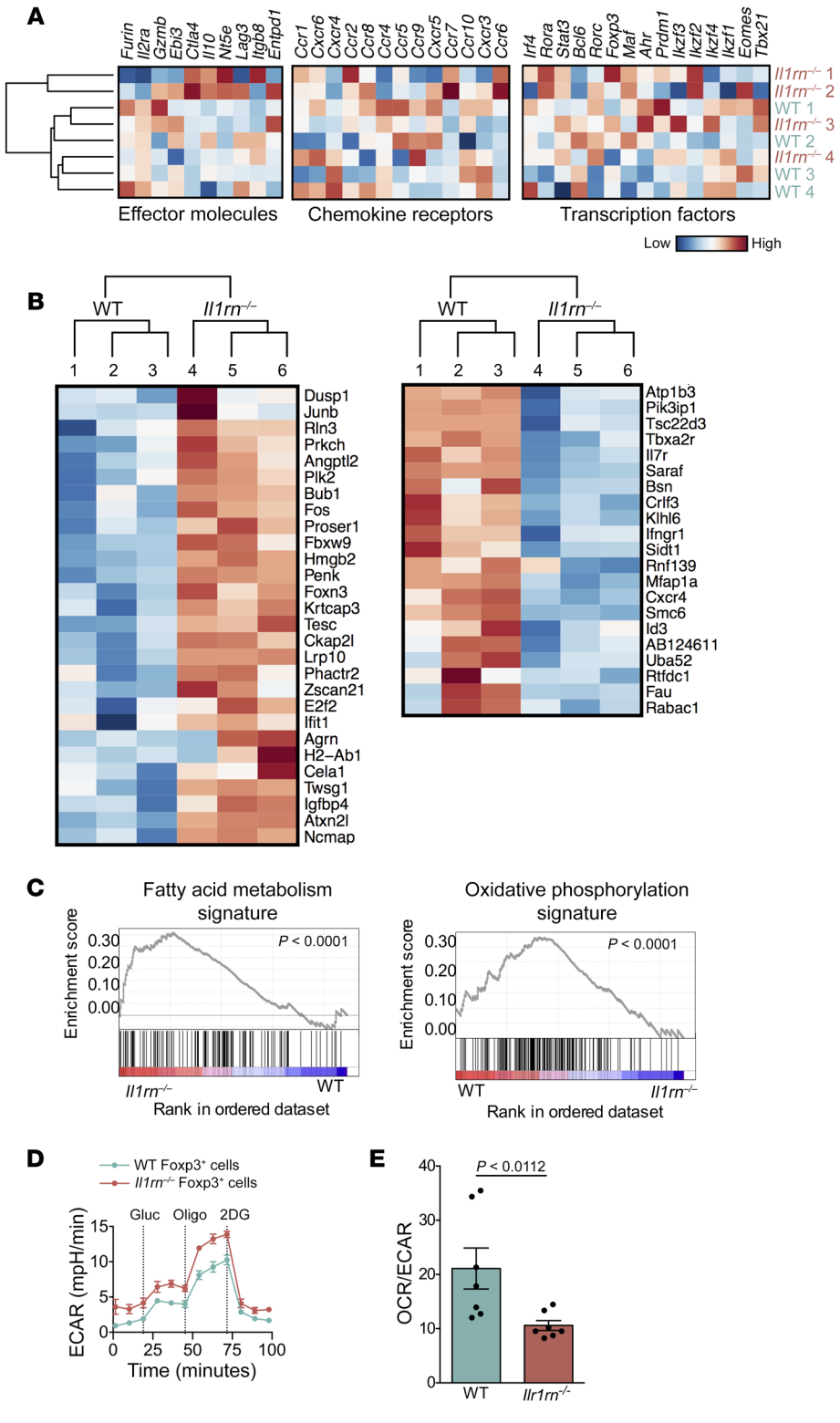

Figure 3. *Il1rn*$^{-/-}$ Tregs exhibit increased glycolysis. (**A** and **C**) CD4^{+}Foxp3^{eGFP+} Treg cells from WT and *Il1rn*$^{-/-}$ mice were sorted and RNA-seq transcriptomes were analyzed. (**A**) Systematic analysis of transcripts encoding the major functional molecules involved in Treg inhibitory function. Comparison is shown of normalized expression values of effector molecules, chemokine receptors, and transcription factors. (**B**) Heatmap of top 50 differentially expressed genes between CD4^{+}Foxp3^{eGFP+} cells sorted from lymph nodes of 3 WT and 3 *Il1rn*$^{-/-}$ Foxp3^{eGFP} animals. (**C**) Overexpression of fatty acid metabolism genes (left) and OxPhos genes (right) in *Il1rn*$^{-/-}$ vs. WT Tregs. (**D** and **E**) WT (1×10^5, $n = 6$) and *Il1rn*$^{-/-}$ (1×10^5, $n = 6$) lymph node CD4^{+}Foxp3^{+} Tregs were equilibrated for 1 hour in unbuffered XF assay medium supplemented with 1 mM sodium pyruvate in an XF24 cell culture microplate. Extracellular acidification rate (ECAR) and oxygen consumption rate (OCR) were measured using an XF24 analyzer (Seahorse Bioscience). Compounds were injected during the assay at the following final concentrations in this glycolysis stress assay: 10 μM glucose, 1 μM oligomycin, and 50 μM 2-deoxyglucose (2DG). (**D**) ECAR ($n = 12$). (**E**) Basal OCR/ECAR ratio ($n = 7$). Data are expressed as mean ± SEM. Statistical significance was determined using 3-way ANOVA (**D** and **E**).

respect to suppression of T cell proliferation, a capacity associated with glycolysis (29).

RANKL^{+} Il1rn$^{-/-}$ Tregs amplify osteoclastogenesis. Protection of bone was the most striking phenotype of early IL-1β blockade, so we sought a connection between Treg expansion and bone erosion. Previous studies found that exTregs express RANKL, which is essential for osteoclast differentiation and implicated in erosions associated with inflammatory arthritis (23). RANKL expression has also been documented in Tregs infiltrating breast tumors (30). Intriguingly, expression of RANKL was substantially greater in *Il1rn*$^{-/-}$ than WT Tregs in both lymph nodes and joints, and increased expression of RANKL by *Il1rn*$^{-/-}$ Tregs was especially marked in synovial tissue (Figure 4, A–F). We examined the osteoclastogenic ability of these cells by culturing WT and

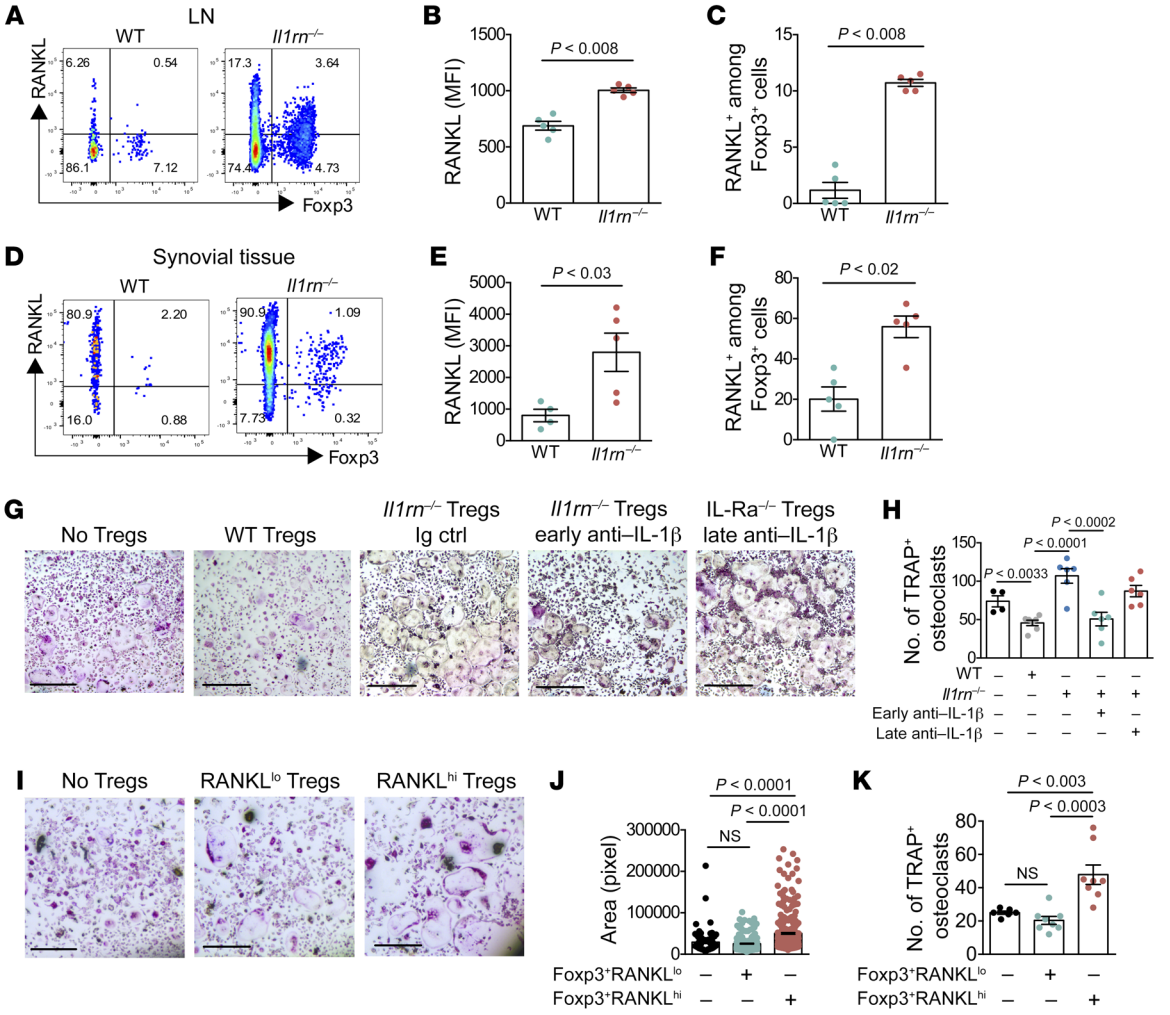

Figure 4. In vivo anti–IL-1β treatment decreases *Il1rn*$^{-/-}$ Treg osteoclastogenic potential and bone erosion. (**A**–**C**) RANKL expression on Foxp3^{eGFP+} T cells from lymph node (LN) by flow cytometry (n = 5 per group). MFI, mean fluorescence intensity. (**D**–**F**) RANKL expression on Foxp3^{eGFP+} T cells from synovial tissue by flow cytometry (n = 5 per group). (**G** and **H**) Sorted Tregs from WT (n = 4) and *Il1rn*$^{-/-}$ treated with anti–IL-1β (n = 5 per group) or Ig control (n = 7) were cocultured with macrophage precursor cells; after 5 days of coculture, cells were stained for tartrate-resistant acid phosphatase (TRAP) and TRAP$^+$ multinucleated cells were counted. Scale bars: 1 mm. (**H**) Number of TRAP$^+$ osteoclasts. (**I**–**K**) Sorted RANKL^{hi} and RANKL^{lo} Foxp3^{eGFP+} Tregs from *Il1rn*$^{-/-}$ mice were cocultured with macrophage precursor cells; after 5 days of coculture, TRAP$^+$ multinucleated cells were measured (surface area) and counted (n = 8 per group). Scale bars: 1 mm. Data are expressed as mean ± SEM. Statistical significance was determined using Mann-Whitney U test (**B** and **D**) or 1-way ANOVA (**F** and **H**).

Il1rn$^{-/-}$ Tregs sorted from lymph nodes with bone marrow–derived monocyte/macrophage precursor cells (BMMs) and enumerating resulting multinucleated tartrate-resistant acid phosphatase–positive (TRAP-positive) osteoclasts. WT Tregs tended to suppress osteoclast formation, consistent with published data (22). By contrast, *Il1rn*$^{-/-}$ Tregs were potently osteoclastogenic, a capacity effectively abrogated by early in vivo IL-1β blockade (Figure 4, G and H). Coculture of BMMs with sorted *Il1rn*$^{-/-}$ Teff cells or *Il1rn*$^{-/-}$ γδ T cells did not induce osteoclast formation (Supplemental Figure 5), highlighting the specificity of osteoclastogenesis by *Il1rn*$^{-/-}$ Tregs. To test the contribution of RANKL, we sorted CD3$^+$ Foxp3^{eGFP+}RANKL^{hi} and CD3$^+$Foxp3^{eGFP+}RANKL^{lo} cells and cocultured them with BMMs. Osteoclastogenesis was restricted to Tregs high in RANKL, as assessed by osteoclast surface area and cell number (Figure 4, I–K). Of note, prior studies had found that blockade of osteoclast formation was dependent on CTLA-4 (22). To further address this point, we purified T cells from WT or *Il1rn*$^{-/-}$ mice and assessed RANKL and CTLA-4 expression. Interestingly, RANKL^{hi} Tregs exhibited low surface CTLA-4, consistent with a pro-osteoclast formation role. Similar results were obtained with T cells stimulated with anti-CD3/anti-CD28 beads for 48 hours (Supplemental Figure 6). Together, these data show that *Il1rn*$^{-/-}$ Tregs overexpress RANKL and acquire an ability to mediate osteoclast development that is absent in their Teff and γδ T counterparts, suggesting that they have become what we believe is a previously undescribed population of O-Tregs potentially contributory to bone erosion in *Il1rn*$^{-/-}$ arthritis.

IL-1β drives osteoclastogenic potential in Tregs. We examined whether the O-Treg phenotype represents a direct effect of IL-1β or an indirect effect mediated by the inflamed arthritic environment. We isolated naive CD4$^+$ cells from Foxp3^{eGFP} animals and cultured them under Treg-polarizing conditions (IL-2 and TGF-β) with or

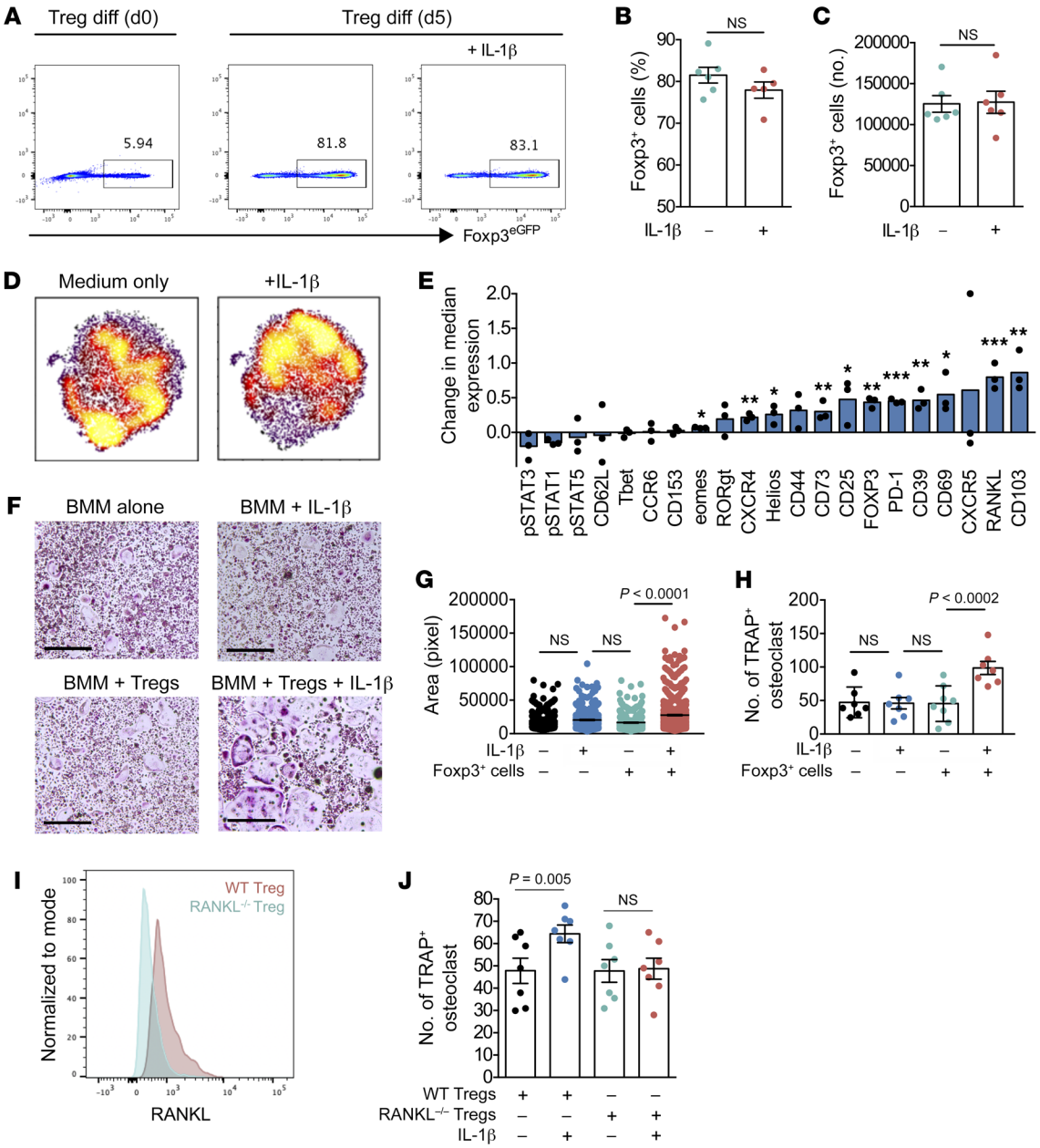

Figure 5. IL-1β confers osteoclastogenic potential to Tregs. CD4+ naive cells from WT mice were isolated and cultured in Treg differentiation media with or without IL-1β (n = 6 per group). (**A**–**C**) Foxp3^{eGFP} expression by flow cytometry after 5 days of Treg differentiation with or without IL-1β (**D** and **E**). iTregs were sorted based on Foxp3^{eGFP} expression and cocultured with bone marrow cells in the presence of M-CSF (20 ng/mL) and RANKL (20 ng/mL) (n = 3 per group). (**D** and **E**) High-dimensional analyses of sorted Foxp3^{eGFP+} iTregs differentiated with or without IL-1β by mass cytometry. (**D**) viSNE plots of iTregs differentiated with or without IL-1β. (**E**) Difference in protein expression between iTregs differentiated with or without IL-1β. (**F**–**H**) Sorted Foxp3^{eGFP+} iTreg cells differentiated with or without IL-1β were cocultured with WT macrophage precursor cells. After 7 days of coculture, cells were stained for tartrate-resistant acid phosphatase (TRAP) and TRAP+ osteoclasts were measured (surface area) and counted. Scale bars: 1 mm. (**I** and **J**) RANKL-deficient Tregs were generated by crossing FoxP3-YFP-Cre mice with *Rankl*$^{fl/fl}$ mice. Littermate mice that do not express FoxP3-YFP-Cre were utilized as WT controls. (**I**) Histogram depicting RANKL expression on WT and *Rankl*$^{-/-}$ Tregs. (**J**) Osteoclastogenic activity of WT and *Rankl*$^{-/-}$ Tregs differentiated in the presence or absence of IL-1β. Data are expressed as mean ± SEM. Statistical significance was determined using Mann-Whitney U test (**B** and **C**), unpaired t test (**F**), or 1-way ANOVA (**G**–**I**). $^*P < 0.01$, $^{**}P < 0.001$, $^{***}P < 0.0001$.

without supplemental IL-1β to form inducible Tregs (iTregs). After 5 days of differentiation, we observed comparable development of Foxp3+ cells irrespective of supplemental IL-1β (Figure 5, A–C). We then studied the expression of Treg markers in a multidimensional manner by mass cytometry, employing tSNE to visualize resulting cells in 2 dimensions on the basis of per-cell phenotypic similarity (Figure 5D). At a population level, iTregs differentiated in the presence of IL-1β showed increased expression of 16 proteins including CD103 (also called ITGAE), RANKL, CD69, and CD39, and a trend toward decreased expression of 5 proteins, including

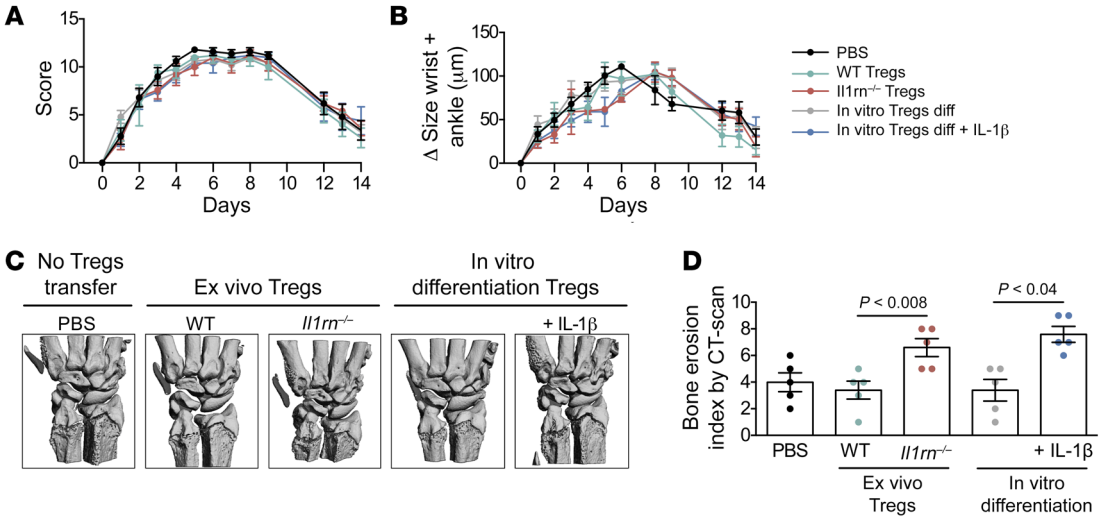

Figure 6. IL-1β–reprogrammed Tregs contribute directly to bone injury under arthritic conditions. (**A** and **D**) BALB/c WT mice were injected with 75 μL i.p. K/BxN serum on days 0 and 2. Sorted CD4$^+$Foxp3^{eGFP+} cells from the lymph nodes of WT (n = 5) or *Il1rn*$^{-/-}$ (n = 5) mice or FOXP3^{eGFP+} iTreg cells differentiated with or without IL-1β (n = 5) (or an equal volume of PBS n = 5) were transferred into BALB/c WT recipient mice 1 day before K/BxN serum injection. (**A**) Arthritis score (0–3/per paw, 0–12 total) and (**B**) ankle and wrist thickening measured by calipers was followed for 14 days after K/BxN injection. (**C**) High-resolution micro-computed tomography (μCT) imaging of wrists from BALB/c WT recipient mice 14 days after K/BxN injection. (**D**) Bone erosion score (0–3 total). Data are expressed as mean ± SEM. Statistical significance was determined using 1-way ANOVA (**A** and **B**) or Mann-Whitney U test (**D**).

p-STAT3 (Figure 5E). The increase in RANKL expression was consistent with our in vivo findings and suggests that IL-1β directly confers osteoclastogenic capacity to Tregs. IL-1β also increased Treg expression of activation markers (CD25, CD39) and markers of suppressive capacity (CD103, CD73, HELIOS) (Figure 5E). We tested the ability of these IL-1β–conditioned Tregs to induce osteoclast differentiation, finding that they had indeed acquired osteoclastogenic capacity compared with iTregs differentiated without IL-1β (Figure 5, F–H). To confirm that osteoclastogenesis is mediated by RANKL, we compared WT and RANKL-deficient Tregs differentiated with and without IL-1β. Interestingly, expression of RANKL was strictly required for IL-1β–driven acquisition of osteoclastogenic capacity (Figure 5I). These findings establish that IL-1β mediates the differentiation of Tregs into O-Tregs capable of inducing osteoclast formation through expression of RANKL.

IL-1β–primed Tregs mediate bone erosion in vivo. To test whether these observations translate into a pathogenic role in vivo, we turned to K/BxN serum transfer arthritis, a model of erosive inflammatory arthritis initiated by transfer of autoantibody-containing serum from arthritic K/BxN F1 mice (31). We isolated CD4$^+$Foxp3$^+$ cells from the lymph nodes of WT and *Il1rn*$^{-/-}$ mice and transferred these cells or an equal volume of diluent into BALB/c WT recipient mice 1 day before K/BxN serum injection. Since K/BxN serum transfer arthritis is independent of T cells, we expected no effect of Treg transfer on arthritis severity, and indeed overall clinical scores and joint swelling were unaffected by Treg transfer (Figure 6, A and B). However, bone erosion as assessed by μCT was markedly and selectively enhanced by *Il1rn*$^{-/-}$ Foxp3$^+$CD4$^+$ T cells (Figure 6, C and D). WT Foxp3$^+$CD4$^+$ iTregs differentiated in the presence of IL-1β exhibited a comparable effect, whereas unconditioned iTregs did not (Figure 6D). These results confirm that IL-1β reprograms Tregs into O-Tregs that mediate bone injury under arthritic conditions.

IL-1β induces an O-Treg population in humans. To assess the human relevance of these results, we isolated naive CD4$^+$ cells from peripheral blood of healthy adult donors and cultured them under iTreg-polarizing conditions, with or without supplemental IL-1β. After 5 days of differentiation, cells were cocultured with peripheral blood CD14$^+$ cells isolated from the same donors to compare their ability to induce osteoclast formation (Figure 7, A and B). iTregs differentiated without IL-1 suppressed osteoclast formation, consistent with previous reports (20–22). By contrast, iTregs differentiated in the presence of IL-1β potently induced the development of TRAP$^+$ osteoclasts (Figure 7, A and B). Thus, IL-1β induces an O-Treg population in humans as well as in mice.

Finally, we analyzed CD4$^+$FOXP3$^+$ T cells from 8 RA and 8 osteoarthritis (OA) synovial tissue samples, using mass cytometry data generated by the Accelerating Medicines Partnership RA/SLE Consortium using an established antibody panel (Supplemental Table 2 and ref. 32). tSNE visualization revealed a population of FOXP3-expressing CD4$^+$ T cells with high RANKL expression clustered together in each of the 16 samples (Figure 7C). Notably, density overlay showed an increase in Tregs expressing a high level of RANKL in RA synovial tissue samples (Figure 7D). Biaxial gating of data from all 16 synovial samples confirmed high expression of RANKL on approximately 10% of synovial CD4$^+$FOXP3$^+$ T cells from RA patients, whereas only approximately 2% of OA synovial Tregs expressed RANKL (Figure 7, E–G). Interestingly, the majority of RA synovial RANKL^{hi} CD4$^+$FOXP3$^+$ T cells coexpressed CD38, HLA-DR, and/or ICOS (Figure 7, C–H), markers of highly suppressive Tregs, although expression of additional markers such as CD127 could not be assessed to further confirm the regulatory status of these cells. Taken together, these results show that human RA tissues include a population with features of the pathogenic O-Tregs that contribute to bone erosion in mice.

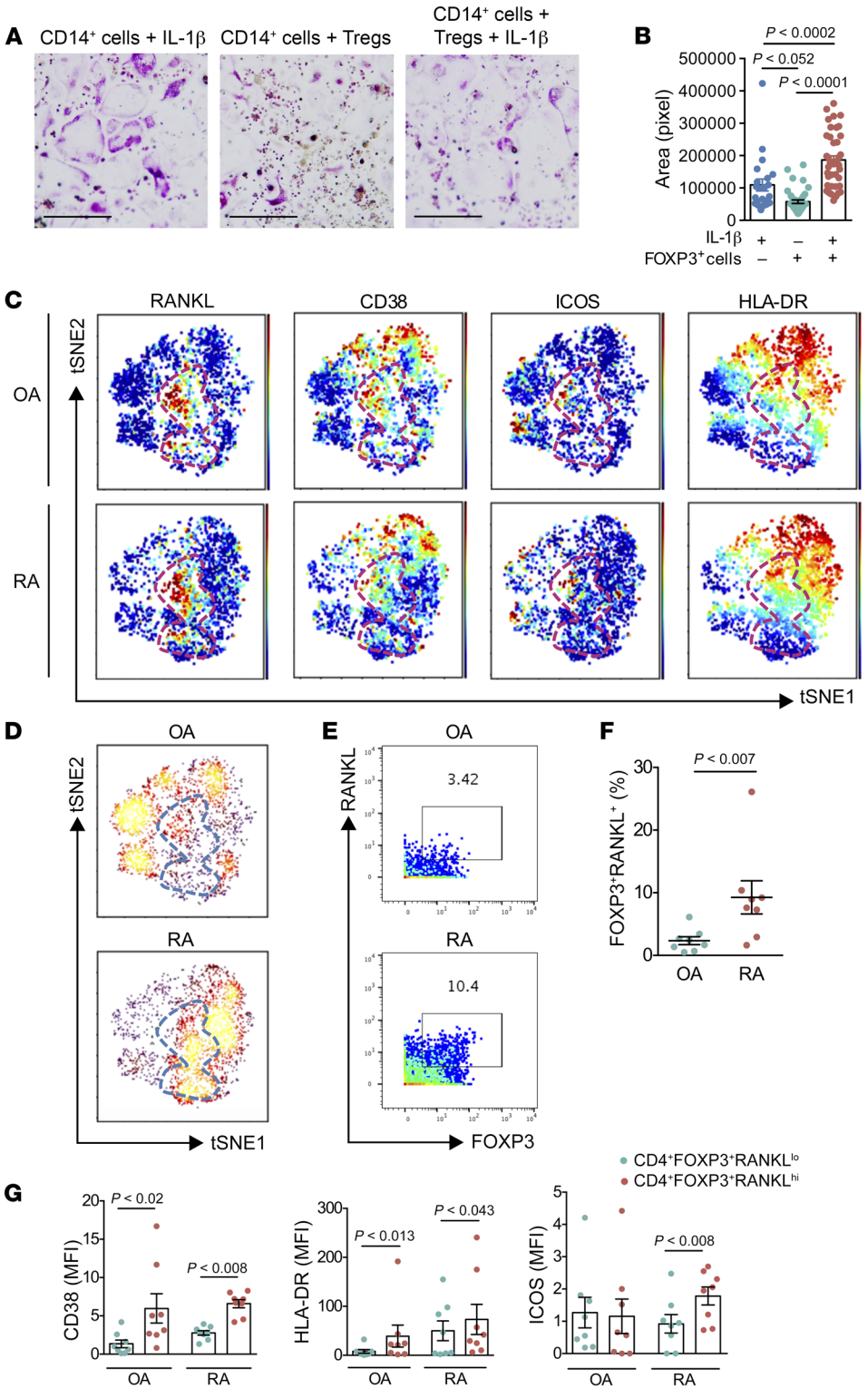

Figure 7. IL-1β induces an osteoclastogenic Treg population in humans. (**A** and **B**) Naive CD4⁺ cells from peripheral blood of healthy adult donors were cultured under iTreg-polarizing conditions, with or without supplemental IL-1β. After 5 days of differentiation, cells were cocultured with peripheral blood CD14⁺ cells isolated from the same donors. After 15 days of coculture, cells were stained for tartrate-resistant acid phosphatase (TRAP) and TRAP⁺ osteoclasts were measured (surface area). Scale bars: 1 mm. (**C**) viSNE plots of synovial CD4⁺FOXP3⁺ T cells from 8 patients with OA and 8 patients with RA. The dashed red outline (in gray in panel **D**) indicates RANKL^{hi} cells. (**D**) viSNE map colored by density. (**E** and **F**) CD4⁺FOXP3⁺RANKL^{hi} T cell frequencies in synovial tissue from RA patients (n = 8) and OA patients (n = 8). (**G**) Expression of indicated proteins by mass cytometry of CD4⁺FOXP3⁺RANKL^{lo} populations and CD4⁺FOXP3⁺RANKL^{hi} cells from 8 patients with OA and 8 patients with RA. MFI, mean fluorescence intensity. Data are expressed as mean ± SEM. Statistical significance was determined using 3-way ANOVA (**B**), Mann-Whitney U test (**F**), or 1-way ANOVA (**G**).

Discussion

Tregs control the activation and differentiation of conventional CD4⁺ T cells and other innate and adaptive immune lineages through a variety of effector mechanisms (15). Further, Tregs modulate nonimmune lineages and serve as agents of tissue homeostasis (33). Here, we identify what we believe to be a new type of stroma-regulating converted Treg, the O-Treg, that is generated through exposure to IL-1β and contributes to bone erosion in inflammatory arthritis.

Plasticity of Tregs is important for their function. For example, expression of the same chemokine receptors as Teff cells allows Tregs to colocalize with their cellular targets (26, 34–36). Acquisition of the ability to elaborate proinflammatory cytokines such as IL-17 and IFN-γ may facilitate a rapid pivot from an immu-

nosuppressive to a defensive role, although these cytokines also have immunoregulatory activity (37–39). By contrast, an inflamed environment or aberrant cytokine signaling may drive development of a population of exFoxp3 cells (sometimes called exTregs) that promote rather than limit immune-mediated disease (23, 40–42). The circumstances under which FOXP3-expressing cells deviate from their usual antiinflammatory role remain incompletely understood (43).

In arthritis, erosive damage to bone is an important determinant of long-term functional outcome (44). Longitudinal studies show that bone erosions occur in more than 60% of RA patients within 2 years of disease onset (45). Although IL-1 blockade has only modest clinical efficacy in RA, treatment attenuates bone erosion; indeed, recombinant IL-1Ra (anakinra) was the first biologic agent shown to protect bone in RA (46, 47). IL-1 blockade is strikingly effective in the highly inflammatory arthritis, systemic juvenile idiopathic arthritis, often abrogating development of chronic joint disease when administered early in the course of illness (48–51). It is therefore important to understand how IL-1 contributes to arthritis, including to bone injury. The present study shows that, in both mice and humans, IL-1β drives Tregs to express RANKL and thereby accelerate osteoclast differentiation. Adoptive transfer confirms that O-Tregs enhance injury to inflamed joints even without aggravating clinical inflammation, and without defined antigen specificity. We find similar cells in human RA joints. Our data therefore define a population pathogenic converted Tregs distinct from the exFoxp3 cells established in other murine contexts (23).

Expression of RANKL by Tregs is not unique to arthritis. Tregs infiltrating breast tumors are the dominant cells expressing RANKL, serving to facilitate metastasis by agonizing RANK on tumor stroma (30). RANKL can be expressed by activated Teff cells, potentially contributing to bone erosion in arthritis and periodontal disease, although at least in antibody-induced murine arthritis fibroblasts remain the key RANKL donor (52–55). The physiological function of Treg RANKL remains unclear. RANK is expressed not only by osteoclasts but also by the medullary thymic epithelial cells (mTECs) responsible for central tolerance, and by lymphoid tissue–inducer (LTi) cells in the lymph nodes; correspondingly, RANK/RANKL signaling is required for normal development of thymic medulla and lymph nodes (56, 57). Intriguingly, Tregs recirculate to the thymus (58), raising the possibility that RANKL-expressing Tregs regulate thymic function, especially since thymic trafficking occurs under the control of CCR6 that we find to be expressed by these cells (59). Treg RANKL could participate in tissue homeostasis through ligation of stromal RANK (30, 33, 60). We speculate that RANKL$^+$ Treg–mediated bone erosion could also be beneficial in some contexts, for example helping to expose or eliminate infected bone in osteomyelitis. Indeed, RANKL-expressing Th17-like exFoxp3 cells facilitate removal of diseased teeth, accelerating resolution of periodontal infections (61). The pathogenic contribution of RANKL-expressing O-Tregs to inflammatory arthritis may thus represent the downside of an adaptation to more pressing existential requirements.

IL-1β has multiple roles in lymphocyte function. It promotes the differentiation of naive CD4$^+$ T cells toward the Th17 lineage and enhances antigen-driven expansion and function in CD4$^+$ and CD8$^+$ T cells (62–66). IL-1 signaling via MyD88 renders Th1 cells resistant to suppression by Tregs (67). Tregs themselves can express the IL-1 receptor IL-1R1, potentially serving as a sink for IL-1, just as they do for IL-2 (26). IL-1β signaling through IL-1R1 attenuates suppressor capacity and promotes expression of IL-17 in Tregs (24, 25, 68, 69). The capacity of IL-1β to induce the O-Treg phenotype further extends the understanding of this cytokine as a modulator of adaptive immunity.

Together, our data indicate that Tregs driven by IL-1β acquire a pathogenic capacity during arthritis, accelerating bone injury even in the absence of transdifferentiation into exTregs. A better understanding of the consequences of chronic inflammation for Treg reprograming will be important to enable the development of safe Treg-mediated therapeutics.

Methods

Mice. *Il1rn*$^{-/-}$ mice were produced as described previously (8). Sex- and age-matched mice, usually at 8 to 12 weeks of age, were used for each experiment. In some experiments, younger mice (3 weeks old) were used as described in the figure legends. IL-1Ra–deficient Foxp3^{eGFP} mice were produced by crossing *Il1rn*$^{-/-}$ mice with BALB/c Foxp3^{eGFP} mice (C.Cg-Foxp3^{tm2Tch}/J) purchased from The Jackson Laboratory (JAX). RANKL-deficient Tregs were generated by crossing FoxP3-YFP-Cre mice with *Rankl*$^{fl/fl}$ mice. Female mice expressing a yellow fluorescent protein/iCre-recombinase fusion protein from the *Foxp3* locus (Foxp3$^{YFP/Cre}$; JAX strain 016959) were crossed with male mice containing loxP sites flanking *Tnfsf11* (*Rankl*$^{fl/fl}$; JAX strain 18978). Their female progeny were crossed with *Rankl*$^{fl/fl}$ again to generate Foxp3$^{YFP/Cre}$ *Rankl*$^{fl/fl}$ mice lacking RANKL on Foxp3-expressing cells. Sex-matched littermate controls that did not express Foxp3$^{YFP/Cre}$ were used for comparison.

Isolation of joint-infiltrating cells. Ankle joints were digested with 1 mg/mL collagenase (MilliporeSigma) in RPMI 1640 (MilliporeSigma) plus 10% fetal bovine serum (FBS, Invitrogen) for 30 minutes at 37°C. The cells were filtered through a cell strainer with a 70 μm nylon mesh (Becton Dickinson) and washed with RPMI 1640 plus 10% FBS.

Arthritis scoring, anti–IL-1β treatment, and serum transfer. Anti–murine IL-1β or isotype-matched IgG (gift from Novartis, Basel, Switzerland) was injected at 5 mg/kg i.p. once per week for 2 weeks either at the weaning (early treatment) or 14 days after (late treatment). Pooled serum (50 μL) from 9- to 11-week-old K/BxN mice was transferred i.p. on day 0 and day 2. Arthritis was graded using a 0 to 12 clinical scale (0 to 3 per paw), as well as by caliper measurement of wrists and ankles, as described previously (70). Histological assessment of ankles was performed on paraffin-embedded sections stained with H&E. Synovial inflammation, cartilage injury, and bone erosion were graded on a 0 to 3 scale (adapted from ref. 71).

Flow cytometry. Antibodies were used at a 1:100 dilution unless otherwise mentioned. The following monoclonal antibodies were purchased from BioLegend: anti–mouse CD196-BV605 (also called CCR6) (29-2L17, catalog number 129819), TCRγδ-FITC (GL3, catalog number 118105), CD254-PE (also called RANKL) (IK22/5, catalog number 510005), CD25-BV650 (PC61, catalog number 102037), CD69-PE/Cy7 (H1.2F3, catalog number 104511), CD3-AF700 (17A2, catalog number 100215), CD4-APC/Cy7 (GK1.5, catalog number 100413), IFN-γ–AF647 (XMG1.2, catalog number 505816), IL-17–PerCP/Cy5.5 (TC11-18H10.1, catalog number 506921), GFP-AF488

(FM264G, catalog number 338007), CD39-PE/Cy7 (Duha59, catalog number 143805), and FOXP3-AF488 (150-D, catalog number 320011). Anti-RORγt–APC (B2D, catalog number 17-6981-82) was purchased from Invitrogen. For intracellular Foxp3 and GFP staining, the Foxp3 Staining Buffer Set (eBioscience) was used. For intracellular cytokine staining, cells were stimulated with a cell activation cocktail without brefeldin A (BioLegend) but with GolgiStop (BD Biosciences) overnight. After washing, cells were stained for surface antigens, fixed with for 10 minutes at room temperature, permeabilized, and stained with monoclonal antibodies against cytokines diluted in Perm/Wash Buffer (BD Biosciences). Flow cytometric analysis was performed by Fortessa with Diva software (BD Biosciences) and analyzed with FlowJo.

T cell isolation and sorting. Single-cell suspensions were obtained from peripheral lymph nodes. $CD4^+$ cells were isolated using immunomagnetic negative selection (Stemcell Technologies). $FoxP3^{eGFP+}$ cells were further isolated by FACS using a FACSAria III (BD Biosciences). The purity of the sorted cells was greater than 99%. Sorted cells were subsequently subjected to cell culture or adoptive transfer experiments. Adoptive transfer was achieved by a retro-orbital vein injection of 5×10^5 cells on the day prior to K/BxN serum transfer. For CellTrace labeling, cells were stained with 5 μM CellTrace Violet (Thermo Fisher Scientific) diluted in PBS at 37°C for 20 minutes.

Treg differentiation in vitro. Single-cell suspensions were obtained from peripheral lymph nodes. Naive $CD4^+$ T cells were isolated using immunomagnetic negative selection (Stemcell Technologies). Naive $CD4^+$ T cells were incubated with reagents included in the CellXVivo Mouse Treg Cell Differentiation Kit (R&D Systems) for 5 days. $FoxP3^{eGFP+}$ cells were further isolated by FACS. Human peripheral blood naive $CD4^+$ T cells were incubated with reagents included in the Human Treg Cell Differentiation Kit (R&D Systems) for 5 days.

In vitro assay of mouse osteoclast differentiation. Primary bone marrow cells were suspended in culture medium (α-MEM containing 10% FBS) supplemented with 10 ng/mL M-CSF (R&D Systems) for 2 days to obtain BMMs. After 3 days, nonadherent cells were replated at a density of 1×10^4 cells/well in 96-well plates and cultured in medium with 10 ng/mL RANKL (R&D Systems) and 20 ng/mL M-CSF for 5 to 7 days. For coculture of BMMs and T cells, BMMs (1×10^4 cells per well) were cultured with sorted T cells (1×10^5 cells per well) in the presence of Dynabeads Mouse T-Activator CD3/CD28 (Thermo Fisher Scientific) for 7 days using a 96-well flat-bottom plate, and $TRAP^+$ multinucleated cells (more than 3 nuclei) were counted and their surface areas measured.

In vitro assay of human osteoclast differentiation. PBMCs from healthy volunteers were isolated by Ficoll/Hypaque density-gradient centrifugation (GE Healthcare). $CD14^+$ cells were isolated using an EasySep Human $CD14^+$ Cell Isolation Kit (Stemcell Technologies). Naive $CD4^+$ T cells were isolated using an EasySep Human Naive $CD4^+$ T Cell Isolation Kit (Stemcell Technologies) and incubated with reagents included in the CellXVivo Human Treg Cell Differentiation Kit for 5 days. $CD14^+$ cells were plated at a density of 1×10^4 cells/well in 96-well plates in α-MEM medium with 10% FBS and 50 ng/mL human M-CSF for 24 hours. After 24 hours, in vitro–differentiated Tregs were added to the osteoclast precursors (1×10^4 cells/well) with 25 ng/mL M-CSF and 40 ng/mL RANKL in the presence of Dynabeads Human T-Activator CD3/CD28 for 15 days, and $TRAP^+$ multinucleated cells (more than 3 nuclei) were counted and their surface areas measured.

μCT. After serial fixation in 4% (4 g/100 mL) paraformaldehyde and 70% (vol/vol) ethanol, knees and ankles were scanned using a μCT 35 (Scanco Medical AG). Scans were conducted in 70% ethanol using a voxel size of 7 μm, x-ray tube potential of 55 kVp, intensity of 0.145 Ma, and integration time of 600 ms. The severity of periarticular ankle erosions was determined blindly on the 3D images using a semiquantitative method. Four sites in the wrist joint were scored: the distal ulnar epiphysis, and the bases of the third, fourth, and fifth metacarpals. Each site received a score of 0 to 3 as described previously (72). The maximal score per paw was 12, and the scores were determined by 2 blinded observers and averaged for a final erosion score. The 3D structures of each knee were assessed using a scoring system from 0 to 3 (0, healthy joint; 1, mild but visible bone destruction at one or more than one site; 2, moderate bone destruction at only one site; 3, moderate bone destruction at more than one site or marked bone destruction at one or more than one site; ref. 73).

Treg suppression assay. $CD4^+Foxp3^{eGFP+}$ Tregs and $CD4^+Foxp3^{eGFP-}$ cells were isolated by FACS. Sorted $CD4^+Foxp3^{eGFP-}$ cells were used as effector cells. The cells were resuspended in RPMI 1640 and labeled with 4 μM CellTrace Violet for 10 minutes at 37°C. Labeling was quenched with complete medium, and the cells were washed twice. Isolated $CD4^+Foxp3^{eGFP+}$ Tregs were added back at a ratio of 1:1. Stimulation was performed using Dynabeads Human T-Activator CD3/CD28 (bead-to-cell ratio 1:1). For proliferation assays, the cell cultures were incubated in complete medium for 3 days.

RNA-seq. RNA was extracted from sorted cells (5×10^4) using a Qiagen RNeasy Micro Kit. RNA-seq was performed using the Smart-Seq2 platform (74, 75). Smart-Seq2 libraries were prepared by the Broad Technology Labs and sequenced by the Joint Biology Consortium–associated Broad Genomics Platform. Transcripts were quantified by the Broad computational pipeline using Cuffquant version 2.2.1 (76). Genes encoding molecules with known roles in Treg localization and trafficking were selected for focused analysis. GSEA was performed using GSEA software v3.0 (Broad Institute) with the Molecular Signatures Database (MSigDB) hallmark gene set collection (77, 78). All original microarray data were deposited in the NCBI's Gene Expression Omnibus database (GEO GSE183254).

Metabolic assays. After FACS isolation, $Foxp3^{eGFP+}$ cells (1×10^5 per well) were seeded onto standard Seahorse 24-well plates coated with Cell-Tak (BD Biosciences) and assayed on a Seahorse XFp Analyzer (Agilent Technologies). Plates were centrifuged at 300*g* for 5 minutes and kept at 37°C overnight. Oxygen consumption rates (OCR) and extracellular acidification rates (ECAR) were measured in XF media with pH adjusted to 7.4. For examining glycolysis, the Glycolysis Stress Test Kit (Seahorse Bioscience) was used with addition of glucose-free nonbuffered Seahorse medium (pH 7.4), including 10 mmol/L glucose, 2 μmol/L oligomycin, and 50 mmol/L 2-deoxyglucose.

Human research. Mass cytometry experiments were performed by the AMP RA/SLE Network. Patients with RA fulfilled the ACR 2010 rheumatoid arthritis classification criteria. Rheumatoid factor and anti-CCP antibody status, C-reactive protein level, and medication usage were obtained by review of electronic medical records. Synovial tissue samples for mass were collected from patients with OA or seropositive RA that were undergoing arthroplasty at the Hospital for Special Surgery, New York or at Brigham and Women's Hospital, Boston.

Synovial tissue analysis. Synovial samples were acquired from discarded arthroplasty tissue. Synovial tissue was isolated by careful dissection, minced, and digested with 100 μg/mL Liberase TL and 100 μg/mL DNase I (both Roche) in RPMI (Life Technologies) for 15 min-

utes, inverting every 5 minutes. Cells were passed through a 70 μm cell strainer, washed, subjected to red blood cell lysis, and cryopreserved in Cryostor CS10 (BioLife Solutions) for batched analyses.

Mass cytometry. Cryopreserved disaggregated synovial cells or PBMCs were thawed into RPMI and 10% FBS (HyClone). Viability was assessed with rhodium for PBMCs and cisplatin (both Fluidigm) for synovial cells. Cells were then washed and stained with primary antibody cocktails at 1:100 dilution. All antibodies were obtained from the Joint Biology Consortium–associated Longwood Medical Area CyTOF Antibody Resource Core. Cells were then washed, fixed, and permeabilized using the Ebioscience Transcription Factor Fix/Perm Buffer for 45 minutes, washed in PBS/1% BSA/0.3% saponin, and then stained for intracellular markers. Cells were refixed in formalin (MilliporeSigma), washed with Milli-Q water, and analyzed using Helios (Fluidigm). Mass cytometry data were normalized using EQ Four Element Calibration Beads (Fluidigm). viSNE analyses were performed using the Barnes-Hut SNE implementation on Cytobank (http://www.cytobank.org). For synovial tissue mass cytometry data, gated $CD4^+Foxp3^+$ T cells were analyzed using all available protein markers, and each synovial tissue sample was analyzed individually to allow for maximal resolution.

Statistics. Unless otherwise stated, comparisons between 2 conditions employed the 2-tailed Wilcoxon matched pairs test and comparisons between 2 groups of mice over time employed the 2-tailed Mann-Whitney *U* test. For measurement and scoring of arthritis over time, we used 2-way ANOVA followed by Bonferroni's post hoc test. Statistical analyses were performed with GraphPad Prism software. A corrected *P* value of less than 0.05 was considered statistically significant.

Study approval. Murine studies were approved by the animal use and care committees of the Dana Farber Cancer Institute and Brigham and Women's Hospital. Research involving human subjects was performed according to the Institutional Review Board at Partners HealthCare, through approved protocols with appropriate written informed consent as required.

Author contributions

AL conceptualized and performed research, analyzed data, and wrote the manuscript. MHC, JS, NNM, JY, MMB, RGB, AW, PYL, RBB, and AM performed research. KW and DAR assisted with human synovial tissue analysis. JAL supervised the mass cytometry experiments. YI provided critical reagents. JFC supervised the osteoclast experiments. PAN conceptualized and supervised research, analyzed data, and wrote the manuscript. All authors edited the manuscript and approved the final version.

Acknowledgments

AL was funded by a Joint Biology Consortium Microgrant (parent grant NIH P30AR070253). MHC was funded by NIH grants T32AI007512 and K12HD052896, and a Rheumatology Research Foundation Scientist Development Award. RGB was funded by a Boehringer Ingelheim Fonds MD Fellowship. JL was funded by a PROMOS scholarship from the German Academic Exchange Service. PYL was funded by NIH grant K08 AR074562. KW and JAL were funded by NIH grant P30AR070253. DAR was funded by the Burroughs Wellcome Fund Career Award for Medical Scientists and National Institute of Arthritis and Musculoskeletal and Skin Diseases (NIAMS) grant K08 AR072791. We acknowledge the AMP RA/SLE Network for the large-scale collection of arthritis patient synovial tissues and mass cytometry data. JFC was funded by NIH grant K08 AR062590 and a Rheumatology Research Foundation K Supplement Award. PAN was funded by NIAMS awards R01AR065538, R01AR075906, R01AR073201, P30AR070253, and R21AR076630; National Heart, Lung, and Blood Institute grant R21HL150575, a Lupus Research Alliance Target Identification in Lupus Grant, the Fundación Bechara, the Arbuckle Family Fund for Arthritis Research, the Samara Jan Turkel Clinical Center for Pediatric Autoimmune Diseases at Boston Children's Hospital, and an investigator-initiated grant from Novartis. Novartis had no input into the design, conduct, or reporting of the studies.

Address correspondence to: Peter A. Nigrovic, Division of Immunology, Boston Children's Hospital, Karp Family Research Building, Room 10211, One Blackfan Circle, Boston, Massachusetts 02115, USA. Phone: 617.905.1373; Email: peter.nigrovic@childrens.harvard.edu.

1. Dinarello CA. The IL-1 family of cytokines and receptors in rheumatic diseases. *Nat Rev Rheumatol*. 2019;15(10):612–632.
2. Mantovani A, et al. Interleukin-1 and related cytokines in the regulation of inflammation and immunity. *Immunity*. 2019;50(4):778–795.
3. Ruscitti P, et al. The role of IL-1β in the bone loss during rheumatic diseases. *Mediators Inflamm*. 2015;2015:782382.
4. Nakamura I, Jimi E. Regulation of osteoclast differentiation and function by interleukin-1. *Vitam Horm*. 2006;74:357–370.
5. Nigrovic PA, et al. Mast cells contribute to initiation of autoantibody-mediated arthritis via IL-1. *Proc Natl Acad Sci U S A*. 2007;104(7):2325–2330.
6. Ji H, et al. Critical roles for interleukin 1 and tumor necrosis factor alpha in antibody-induced arthritis. *J Exp Med*. 2002;196(1):77–85.
7. Staite ND, et al. Induction of an acute erosive monarticular arthritis in mice by interleukin-1 and methylated bovine serum albumin. *Arthritis Rheum*. 1990;33(2):253–260.
8. Horai R, et al. Development of chronic inflammatory arthropathy resembling rheumatoid arthritis in interleukin 1 receptor antagonist-deficient mice. *J Exp Med*. 2000;191(2):313–320.
9. Akitsu A, et al. IL-1 receptor antagonist-deficient mice develop autoimmune arthritis due to intrinsic activation of IL-17-producing CCR2(+)Vγ6(+) γδ T cells. *Nat Commun*. 2015;6:7464.
10. Horai R, et al. TNF-alpha is crucial for the development of autoimmune arthritis in IL-1 receptor antagonist-deficient mice. *J Clin Invest*. 2004;114(11):1603–1611.
11. Nakae S, et al. IL-17 production from activated T cells is required for the spontaneous development of destructive arthritis in mice deficient in IL-1 receptor antagonist. *Proc Natl Acad Sci U S A*. 2003;100(10):5986–5990.
12. Koenders MI, et al. Interleukin-1 drives pathogenic Th17 cells during spontaneous arthritis in interleukin-1 receptor antagonist-deficient mice. *Arthritis Rheum*. 2008;58(11):3461–3470.
13. Ikeda S, et al. Excess IL-1 signaling enhances the development of Th17 cells by downregulating TGF-β-induced Foxp3 expression. *J Immunol*. 2014;192(4):1449–1458.
14. Chang MH, Nigrovic PA. Antibody-dependent and -independent mechanisms of inflammatory arthritis. *JCI Insight*. 2019;4(5):e125278.
15. Georgiev P, et al. Regulatory T cells: the many faces of Foxp3. *J Clin Immunol*. 2019;39(7):623–640.
16. Brunkow ME, et al. Disruption of a new forkhead/winged-helix protein, scurfin, results in the fatal lymphoproliferative disorder of the scurfy mouse. *Nat Genet*. 2001;27(1):68–73.
17. Kim JM, et al. Regulatory T cells prevent catastrophic autoimmunity throughout the lifespan of mice. *Nat Immunol*. 2007;8(2):191–197.
18. Cao D, et al. Isolation and functional characterization of regulatory $CD25^{bright}CD4^+$ T cells from the target organ of patients with rheumatoid arthritis. *Eur J Immunol*. 2003;33(1):215–223.
19. Mottonen M, et al. $CD4^+$ $CD25^+$ T cells with the phenotypic and functional characteristics of regulatory T cells are enriched in the synovial fluid

of patients with rheumatoid arthritis. *Clin Exp Immunol*. 2005;140(2):360–367.
20. Kelchtermans H, et al. Activated CD4+CD25+ regulatory T cells inhibit osteoclastogenesis and collagen-induced arthritis. *Ann Rheum Dis*. 2009;68(5):744–750.
21. Kim YG, et al. Human CD4+CD25+ regulatory T cells inhibit the differentiation of osteoclasts from peripheral blood mononuclear cells. *Biochem Biophys Res Commun*. 2007;357(4):1046–1052.
22. Zaiss MM, et al. Treg cells suppress osteoclast formation: a new link between the immune system and bone. *Arthritis Rheum*. 2007;56(12):4104–4112.
23. Komatsu N, et al. Pathogenic conversion of Foxp3+ T cells into TH17 cells in autoimmune arthritis. *Nat Med*. 2014;20(1):62–68.
24. Koenen HJ, et al. Human CD25highFoxp3pos regulatory T cells differentiate into IL-17-producing cells. *Blood*. 2008;112(6):2340–2352.
25. Li L, et al. IL-1β-mediated signals preferentially drive conversion of regulatory T cells but not conventional T cells into IL-17-producing cells. *J Immunol*. 2010;185(7):4148–4153.
26. Chaudhry A, et al. CD4+ regulatory T cells control TH17 responses in a Stat3-dependent manner. *Science*. 2009;326(5955):986–991.
27. Rubtsov YP, et al. Stability of the regulatory T cell lineage in vivo. *Science*. 2010;329(5999):1667–1671.
28. Feuerer M, et al. Genomic definition of multiple ex vivo regulatory T cell subphenotypes. *Proc Natl Acad Sci U S A*. 2010;107(13):5919–5924.
29. Gerriets VA, et al. Foxp3 and Toll-like receptor signaling balance T_{reg} cell anabolic metabolism for suppression. *Nat Immunol*. 2016;17(12):1459–1466.
30. Tan W, et al. Tumour-infiltrating regulatory T cells stimulate mammary cancer metastasis through RANKL-RANK signalling. *Nature*. 2011;470(7335):548–553.
31. Korganow AS, et al. From systemic T cell self-reactivity to organ-specific autoimmune disease via immunoglobulins. *Immunity*. 1999;10(4):451–461.
32. Zhang F, et al. Defining inflammatory cell states in rheumatoid arthritis joint synovial tissues by integrating single-cell transcriptomics and mass cytometry. *Nat Immunol*. 2019;20(7):928–942.
33. Panduro M, et al. Tissue Tregs. *Annu Rev Immunol*. 2016;34:609–633.
34. Kleinewietfeld M, et al. CCR6 expression defines regulatory effector/memory-like cells within the CD25(+)CD4+ T-cell subset. *Blood*. 2005;105(7):2877–2886.
35. Duhen T, et al. Functionally distinct subsets of human FOXP3+ Treg cells that phenotypically mirror effector Th cells. *Blood*. 2012;119(19):4430–4440.
36. Koch MA, et al. The transcription factor T-bet controls regulatory T cell homeostasis and function during type 1 inflammation. *Nat Immunol*. 2009;10(6):595–602.
37. Beriou G, et al. IL-17-producing human peripheral regulatory T cells retain suppressive function. *Blood*. 2009;113(18):4240–4249.
38. Koenecke C, et al. IFN-γ production by allogeneic Foxp3+ regulatory T cells is essential for preventing experimental graft-versus-host disease. *J Immunol*. 2012;189(6):2890–2896.
39. Esplugues E, et al. Control of TH17 cells occurs in the small intestine. *Nature*. 2011;475(7357):514–518.
40. Zhou X, et al. Instability of the transcription factor Foxp3 leads to the generation of pathogenic memory T cells in vivo. *Nat Immunol*. 2009;10(9):1000–1007.
41. Bailey-Bucktrout SL, et al. Self-antigen-driven activation induces instability of regulatory T cells during an inflammatory autoimmune response. *Immunity*. 2013;39(5):949–962.
42. Massoud AH, et al. An asthma-associated IL4R variant exacerbates airway inflammation by promoting conversion of regulatory T cells to TH17-like cells. *Nat Med*. 2016;22(9):1013–1022.
43. Hori S. Lineage stability and phenotypic plasticity of Foxp3+ regulatory T cells. *Immunol Rev*. 2014;259(1):159–172.
44. Welsing PM, et al. Minimal clinically important difference in radiological progression of joint damage. A definition based on patient perspective. *J Rheumatol*. 2006;33(3):501–507.
45. van der Heijde DM. Joint erosions and patients with early rheumatoid arthritis. *Br J Rheumatol*. 1995;34(suppl 2):74–78.
46. Bresnihan B, et al. Treatment of rheumatoid arthritis with recombinant human interleukin-1 receptor antagonist. *Arthritis Rheum*. 1998;41(12):2196–2204.
47. Jiang Y, et al. A multicenter, double-blind, dose-ranging, randomized, placebo-controlled study of recombinant human interleukin-1 receptor antagonist in patients with rheumatoid arthritis: radiologic progression and correlation of Genant and Larsen scores. *Arthritis Rheum*. 2000;43(5):1001–1009.
48. Ruperto N, et al. Two randomized trials of canakinumab in systemic juvenile idiopathic arthritis. *N Engl J Med*. 2012;367(25):2396–2406.
49. Nigrovic PA, et al. Anakinra as first-line disease-modifying therapy in systemic juvenile idiopathic arthritis: report of forty-six patients from an international multicenter series. *Arthritis Rheum*. 2011;63(2):545–555.
50. Nigrovic PA. Review: is there a window of opportunity for treatment of systemic juvenile idiopathic arthritis? *Arthritis Rheumatol*. 2014;66(6):1405–1413.
51. Ter Haar NM, et al. Treatment to target using recombinant interleukin-1 receptor antagonist as first-line monotherapy in new-onset systemic juvenile idiopathic arthritis: results from a five-year follow-up study. *Arthritis Rheumatol*. 2019;71(7):1163–1173.
52. Wong BR, et al. TRANCE is a novel ligand of the tumor necrosis factor receptor family that activates c-Jun N-terminal kinase in T cells. *J Biol Chem*. 1997;272(40):25190–25194.
53. Kong YY, et al. Activated T cells regulate bone loss and joint destruction in adjuvant arthritis through osteoprotegerin ligand. *Nature*. 1999;402(6759):304–309.
54. Kawai T, et al. B and T lymphocytes are the primary sources of RANKL in the bone resorptive lesion of periodontal disease. *Am J Pathol*. 2006;169(3):987–998.
55. Danks L, et al. RANKL expressed on synovial fibroblasts is primarily responsible for bone erosions during joint inflammation. *Ann Rheum Dis*. 2016;75(6):1187–1195.
56. Dougall WC, et al. RANK is essential for osteoclast and lymph node development. *Genes Dev*. 1999;13(18):2412–2424.
57. Hikosaka Y, et al. The cytokine RANKL produced by positively selected thymocytes fosters medullary thymic epithelial cells that express autoimmune regulator. *Immunity*. 2008;29(3):438–450.
58. Thiault N, et al. Peripheral regulatory T lymphocytes recirculating to the thymus suppress the development of their precursors. *Nat Immunol*. 2015;16(6):628–634.
59. Cowan JE, et al. Aire controls the recirculation of murine Foxp3+ regulatory T-cells back to the thymus. *Eur J Immunol*. 2018;48(5):844–854.
60. Ahern E, et al. Roles of the RANKL-RANK axis in antitumour immunity - implications for therapy. *Nat Rev Clin Oncol*. 2018;15(11):676–693.
61. Tsukasaki M, et al. Host defense against oral microbiota by bone-damaging T cells. *Nat Commun*. 2018;9(1):701.
62. Acosta-Rodriguez EV, et al. Interleukins 1beta and 6 but not transforming growth factor-beta are essential for the differentiation of interleukin 17-producing human T helper cells. *Nat Immunol*. 2007;8(9):942–949.
63. Chung Y, et al. Critical regulation of early Th17 cell differentiation by interleukin-1 signaling. *Immunity*. 2009;30(4):576–587.
64. Ben-Sasson SZ, et al. IL-1 acts directly on CD4 T cells to enhance their antigen-driven expansion and differentiation. *Proc Natl Acad Sci U S A*. 2009;106(17):7119–7124.
65. Zielinski CE, et al. Pathogen-induced human TH17 cells produce IFN-gamma or IL-10 and are regulated by IL-1beta. *Nature*. 2012;484(7395):514–518.
66. Ben-Sasson SZ, et al. IL-1 enhances expansion, effector function, tissue localization, and memory response of antigen-specific CD8 T cells. *J Exp Med*. 2013;210(3):491–502.
67. Schenten D, et al. Signaling through the adaptor molecule MyD88 in CD4+ T cells is required to overcome suppression by regulatory T cells. *Immunity*. 2014;40(1):78–90.
68. Deknuydt F, et al. IL-1beta and IL-2 convert human Treg into T(H)17 cells. *Clin Immunol*. 2009;131(2):298–307.
69. Alvarez F, et al. The alarmins IL-1 and IL-33 differentially regulate the functional specialisation of Foxp3+ regulatory T cells during mucosal inflammation. *Mucosal Immunol*. 2019;12(3):746–760.
70. Nigrovic PA, et al. C5a receptor enables participation of mast cells in immune complex arthritis independently of Fcγ receptor modulation. *Arthritis Rheum*. 2010;62(11):3322–3333.
71. Delgado M, et al. Vasoactive intestinal peptide prevents experimental arthritis by downregulating both autoimmune and inflammatory components of the disease. *Nat Med*. 2001;7(5):563–568.
72. O'Brien W, et al. RANK-independent osteoclast formation and bone erosion in inflammatory arthritis. *Arthritis Rheumatol*. 2016;68(12):2889–2900.
73. Fatima F, et al. Radiological features of experimental staphylococcal septic arthritis by micro computed tomography scan. *PLoS One*.

2017;12(2):e0171222.
74. Picelli S, et al. Smart-seq2 for sensitive full-length transcriptome profiling in single cells. *Nat Methods*. 2013;10(11):1096–1098.
75. Trombetta JJ, et al. Preparation of single-cell RNA-Seq libraries for next generation sequencing. *Curr Protoc Mol Biol*. 2014;107:4.22.1–17.
76. Trapnell C, et al. Differential gene and transcript expression analysis of RNA-seq experiments with TopHat and Cufflinks. *Nat Protoc*. 2012;7(3):562–578.
77. Liberzon A, et al. The Molecular Signatures Database (MSigDB) hallmark gene set collection. *Cell Syst*. 2015;1(6):417–425.
78. Subramanian A, et al. Gene set enrichment analysis: a knowledge-based approach for interpreting genome-wide expression profiles. *Proc Natl Acad Sci U S A*. 2005;102(43):15545–15550.